Mine Closure 2026 – AB Fourie, G Boggs, J Heyes & M Tibbett (eds)

doi:10.36487/ACG_repo/2615_135

Fibre reinforcement to improve tensile strength and desiccation behaviour of red mud at reduced moisture contents for tailings storage facility closure

Sebastian Quintero Olaya [a,*], Chenming Zhang [a], Yuefeng Yang [a], Sai Ashrith Moturi [a], David Williams [a]

[a] *School of Civil Engineering, The University of Queensland, Australia*

Abstract

Red mud (bauxite residue) tailings is caustic, clayey silt-sized material characterised by high water retention, slow consolidation and low strength development during discharge into tailings storage facilities (TSFs), resulting in ongoing operational challenges and increased closure complexity. As red mud TSFs progress towards closure and rehabilitation, these characteristics can translate into elevated porewater pressures, limited strength gain and long-term instability risks, including groundwater levels remaining close to the surface.

This study investigates the use of polypropylene (PP) and high-density polyethylene (HDPE) fibre reinforcement to improve the mechanical behaviour of red mud at reduced moisture contents (MCs) relevant to closure and rehabilitation phases. These fibre types are known to exhibit long-term chemical stability in highly alkaline red mud environments. Three fibre types were incorporated into red mud over a range of MCs, with testing focused on conditions close to the optimum moisture content (OMC). Unconfined compressive strength (UCS) and Brazilian tensile strength (BTS) tests were undertaken to quantify strength enhancement attributable to fibre inclusion, with particular attention given to tensile behaviour and crack development during desiccation.

The fibre reinforcement approach was evaluated using shrinkage–moisture relationships and tensile strength testing, providing a mechanistic assessment of crack resistance and strength retention under desiccation conditions. The results indicate that fibre reinforcement contributes to increased tensile and compressive strength by around 2 times the unreinforced red mud and promotes improved post-cracking behaviour as the MC decreases.

Fibre addition was observed to enhance air entry development and to limit crack propagation during desiccation, resulting in a more stable material fabric at lower moisture contents. These findings suggest that fibre reinforcement may provide a viable pathway to improve red mud strength and desiccation performance with a void ratio decrease by up to 6% at liquid limit (LL), thereby reducing closure stage stability risks and supporting more robust rehabilitation outcomes for red mud TSFs.

Keywords: *red mud, fibre reinforcement, tensile strength, tailings storage, shrinkage*

1 Introduction

All tailings types present challenges during storage, requiring careful design, monitoring and geotechnical understanding of material behaviour (Australian Government 2016). Among the various tailings streams, red mud is ranked as one of the largest and most persistent mine wastes globally (Luckeneder et al. 2021) and has featured prominently in Australian mining operations (Olaya et al. 2023).

Red mud, commonly produced through the Bayer process (Pradhan et al. 2024; Svobodova-Sedlackova et al. 2024), exhibits geotechnical and geochemical characteristics that make long-term storage and closure

* Corresponding author. Email address: s.quintero@uq.edu.au

challenging. Fresh red mud is typically highly alkaline, with pH values exceeding 12, while sea water neutralised residues commonly exhibit pH values of approximately 10 (Ranabhat et al. 2025; Zhang et al. 2019). Geotechnically, red mud is generally composed of fine clay/silt-sized particles with low permeability and slow consolidation, resulting in a water-retentive material that develops strength gradually under self-weight settlement and loading. These characteristics lead to soft, low-trafficability surfaces and limited shear and tensile strength, restricting accessibility, desiccation efficiency and revegetation potential during rehabilitation (Williams 2015; Zhang et al. 2025).

While tailings improvement techniques such as thickening paste, mud farming and dewatering can promote surface drying and consolidation (Williams 2021), they may not fundamentally improve the tensile behaviour of red mud. Tensile strength has received comparatively limited attention in TSF-based research (Tian et al. 2024). As MC decreases, capillary forces develop within unsaturated tailings (Narvaez et al. 2015). Under these conditions, previous studies have shown that red mud can undergo volumetric shrinkage of up to 40% from its original size (Ranabhat et al. 2023), promoting desiccation, cracking and formation of preferential flow pathways (Ranabhat et al. 2023; Vo et al. 2019). Such cracking can reduce strength and adversely affect long-term TSF performance (Luo et al. 2023; Mishra et al. 2019), particularly where water flow becomes dominated by fracture pathways rather than by intrinsic material permeability (Arredondo et al. 2020).

Fibre reinforcement is widely used to improve tensile strength, ductility and crack resistance in soils, concrete and tailings materials (Consoli et al. 1999; Cristelo et al. 2017; Yi et al. 2015; Zafar et al. 2023; Zollo 1997). In mining applications, fibre reinforcement has also demonstrated improved crack control and mechanical behaviour in cemented tailings materials (Chen et al. 2020; Guo et al. 2024; Zou et al. 2025). However, direct reinforcement of uncemented tailings, particularly red mud, has received comparatively limited attention, specially under TSF desiccation and closure conditions where cracking and long-term stability are critical. Only a small group of studies has considered investigating a direct interaction between fibres and tailings within a specific context of TSF desiccation (Festugato et al. 2015; Girao & Casagrande 2019; Liu et al. 2021; Olaya et al. 2023; Olaya et al. 2020).

Fibres have been shown to modify desiccation behaviour by restraining shrinkage and maintaining matrix integrity as this matrix dries (Bai et al. 2026; Chaduvula et al. 2017). Although this may delay air entry and reduce drying rates, desiccation occurs more uniformly through the material rather than through connected cracks (Arredondo et al. 2020; Luo et al. 2023). Existing studies on fibre-reinforced red mud have largely studied cemented systems intended as construction material alternatives (Wu et al. 2024). However, research that evaluates fibre reinforcement directly within uncemented red mud under desiccation conditions relevant to TSF closure and rehabilitation, is limited. In particular, the influence of fibre reinforcement to tensile behaviour, shrinkage driven cracking and post-crack response of red mud at low moisture contents remains poorly understood. From a TSF closure perspective, this represents an important knowledge gap, as uncontrolled cracking can promote preferential flow pathways and reduce long-term stability.

To address this gap, the present study investigates the contribution of plastic fibre reinforcement to red mud behaviour under low moisture conditions representative of late-stage TSF desiccation towards to end of production and rehabilitation. High-density polyethylene (HDPE) and polypropylene (PP) fibres were selected due to their chemical stability, mechanical robustness and resistance to degradation in highly alkaline and abrasive environments such as red mud (Stakne 2003). This study combines unconfined compressive strength (UCS) and Brazilian tensile strength (BTS) testing at conditions near the optimum moisture content (OMC), with volumetric shrinkage and crack observations to assess the influence of fibre addition on strength development, desiccation behaviour and crack resistance. Through this approach, the study aims to evaluate whether fibre reinforcement can improve the tensile response and post-cracking behaviour of red mud at low moisture contents, thereby enhancing its suitability for long-term TSF closure and rehabilitation.

2 Materials and testing methodology

2.1 Materials used

Sea water neutralised red mud from southeast Queensland was used as the primary material in this study. This mining waste was selected due to its relevance, geotechnical complexity and popularity to the Australian mining industry, its geotechnical and geochemical complex nature and its known cementitious proclivity (Quintero et al. 2017).

Three types of plastic fibres were investigated. These comprised 2 PP fibres, referred to as black fibres (BF) and red fibres (RF) based on their physical appearance, and HDPE fibre, referred to as white fibre (WF). All fibres were manufactured by Texo ReoCo. Figure 1 shows the physical appearance of the materials used in this study.

(a) (b)

Figure 1 Materials used in this study; (a) Red mud prepared at plastic limit; (b) Three types of plastic fibres (black and red are polypropylene and white is high-density polyethylene)

2.2 Testing methodology

2.2.1 Individual tests on red mud and fibre

Table 1 presents the particle size distribution determined using sieve and hydrometer, Atterberg limits, pH and specific gravity tests conducted on red mud. X-ray diffraction analysis was also performed to characterise the mineralogical composition. The principal mineral phases identified are summarised in Table 1.

Table 1 Geotechnical and geochemical characterisation of red mud

Parameter	Value
Liquid limit, LL (%)	47.9
Plastic limit, PL (%)	33.5
Plasticity index, PI (%)	14.4
Sand grain portion (%, 0.075–4.75 mm)	3.22
Silt grain portion (%, 0.002–0.075 mm)	32.27
Clay grain portion (%, <0.002 mm)	64.5
Diameter at 50%, D50 (µm)	3.01
Specific gravity, SG	2.89
pH	9.65
Hematite, Fe_2O_3 (%)	36
Nosean, $Na_8Al_6Si_6O_{24}(SO_4)$ (%)	18
Calcite, $CaCO_3$ (%)	2
Quartz, SiO_2 (%)	2
Kaolinite, $Al_2Si_2O_5(OH)_4$ (%)	2
Anatase, TiO_2 (%)	2
Boehmite, γ-AlO(OH) (%)	2
Rutile, TiO_2 (%)	1
Zircon, $ZrSiO_4$ (%)	1
Gibbsite, γ-Al $(OH)_3$ (%)	<1
Amorphous (%)	38

Table 2 summarises the geometrical, physical and mechanical properties of the 3 fibre types.

In addition to their geometrical and mechanical properties, surface roughness measurements were conducted using a Zeta 300 optical profiler. Measurements were obtained at 3 separate sites per fibre (100 × magnification with a minimum z-step size of 12 nm). Linear roughness (R_a) and area roughness (S_a) were measured on each fibre type.

Surface roughness – often referred to as asperity (Martinez & Frost 2017) – was quantified to provide a supplementary context for red mud–fibre interaction mechanisms, particularly under tensile strength. Comparable approaches have been reported for soil, tailings and cemented geomaterials interacting with external reinforcements such as fibres, geotextile and steel (Martinez & Frost 2017; Shaia & Abuel-Naga 2014; Thomason 2023; Vangla & Latha Gali 2016).

Table 2 Physical and mechanical properties of the plastic fibres

Parameter	Value		
	BF	RF	WF
Original length (mm)	30	45	35
Cross-section(major *a* × minor *b*)(μm)	100 × 55	100 × 90	87 × 60
Equivalent diameter (μm)	Approx. 74	Approx. 95	Approx. 72
Density (g/cm^3)	0.91	0.88	0.94
Tensile strength (MPa)	496.07	4,741.86	4,607.82
Average area roughness, S_a (μm)	0.15	0.29	0.32
Average linear roughness, R_a (μm)	0.09	0.32	0.22

The fibre density relative to the specific gravity of red mud (Table 1) suggests that fibres may exhibit initial buoyancy during red mud settlement. However, previous studies indicate that a significant proportion of fibres become entrained within the matrix due to consolidation under the self-weight of red mud. Fibres remaining near the surface are progressively incorporated as supernatant water evaporates, allowing continued fibre–red mud interaction (Olaya et al. 2020). R_a in Table 2 is of particular attention in this study. Based on fibre–soil interfacial interaction mechanisms, the reinforcement benefit in fibre-reinforced soils has been shown to exhibit a linear relationship with fibre–soil interfacial strength (Tang et al. 2016). This mechanistic relationship is directly relevant to long-term red mud behaviour in TSFs, where the material desiccation is inevitable and required throughout the duration of the TSF life cycle.

As red mud desiccates, tensile stresses develop as a result of increasing matric suction and capillary forces. These stresses, together with geometric confinement arising from volumetric shrinkage, govern the evolution of tensile strength and the initiation and propagation of desiccation cracks (Ranabhat et al. 2025; Tian et al. 2023). Fibre surface roughness influences the efficiency of crack bridging by enhancing fibre–matrix interlocking and pull-out resistance, thereby restraining crack opening and uncontrolled crack propagation (Kodikara & Costa 2013). The variations in R_a per fibre type indicate meaningful differences in surface roughness.

2.2.2 Fibre-reinforced red mud tests

The experimental program was designed to investigate the tensile behaviour and desiccation response of red mud under low moisture conditions and high dry density values. In particular, the study seeks to address whether red mud exhibits measurable tensile strength below LL value, whether tensile resistance can be enhanced through fibre reinforcement, and whether fibre surface roughness contributes to crack bridging and crack resistance during drying.

To address these questions, fibre-reinforced red mud specimens were prepared a 1% plastic fibre addition by dry mass, selected based on previous studies demonstrating effective reinforcement at low fibre contents while maintaining workability and avoiding fibre clustering. The program combined UCS, BTS, volumetric shrinkage, compaction, mineralogical and surface roughness data to evaluate fibre–red mud interaction mechanisms.

This integrated approach allows the relationship between shrinkage, cracking and tensile behaviour to be assessed under moisture conditions relevant to long-term TSF closure. In addition, the mineralogy exhibited in Table 1 provides context for the intrinsic shrinkage susceptibility of red mud, while shrinkage curves for each fibre-reinforced sample can give a measurable approach to assess whether fibres can compensate for these material tendencies.

Standard laboratory procedures were followed throughout the experimental program. Compaction characteristics were determined using standard compaction testing to define OMC and maximum dry density (MDD). These values were used as reference parameters for material densification and as a reliable mechanism for sample preparation. UCS and BTS tests were conducted using a servo-controlled loading frame under quasi-static loading conditions at 4 mm/min for UCS tests and a rate of 1 mm/min for BTS tests. Volumetric shrinkage was measured in accordance with ASTM procedures, with shrinkage strain interpreted using established volumetric shrinkage curve (Fredlund et al. 2006) These tests were selected to characterise strength development, crack resistance and desiccation behaviour under closure-relevant moisture conditions.

3 Test results and discussion

3.1 Standard compaction tests

Compaction test results for unreinforced red mud (control) and fibre-reinforced red mud are presented in Figure 2. The results indicate that the inclusion of fibres at a dosage of 1% by dry mass does not significantly affect the MDD of red mud. When normalised against the unreinforced material, the MDD values for specimens reinforced with BF, RF and WF correspond to 98.92%, 102.0% and 99.83%, respectively. This demonstrates that the MDD of red mud remains largely unchanged by fibre addition, with a small increase observed for specimens incorporating RF.

Similarly, the OMC of the fibre-reinforced specimens shows limited variations as well, with normalised OMC values of 95.65%, 102.90% and 79.71% for BF, RF and WF, respectively. Among the 3 fibre types, WF produces the most pronounced change, with an OMC approximately 20% lower than that of the unreinforced material.

From a desiccation perspective, this reduction in OMC suggests that red mud reinforced with WF would need to undergo greater moisture loss to reach its optimum compaction state compared to the unreinforced material. While this may increase drying rates under field conditions, the largely unchanged MDD indicates that fibre addition does not compromise the maximum achievable density of the material. This behaviour is relevant from a TSF management perspective, where compaction efficiency, strength development and crack control must be balanced.

For consistency across the experimental program, the OMC and MDD determined from the unreinforced red mud were adopted for the preparation of all specimens in this study.

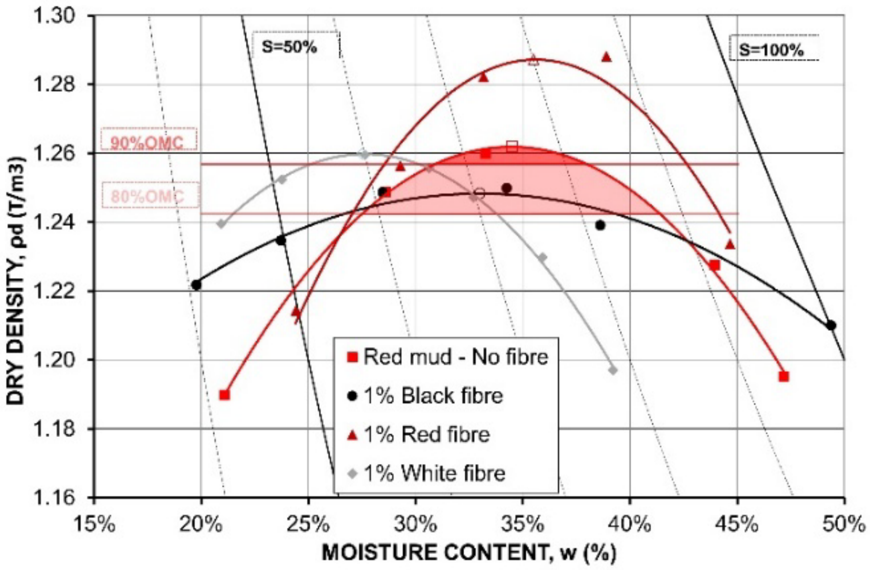

Figure 2 Standard compaction test results for unreinforced and fibre-reinforced red mud

3.2 Shrinkage behaviour test results

All specimens for volumetric shrinkage tests were conducted using moulds with a nominal diameter of 60 mm and a height of 20 mm. The target MC of the unreinforced red mud of 98% was the equivalent moisture to full saturation (S_r = 100%).

Each test was carried out controlling the rate of evaporation of all 4 specimens to collect the largest amount of data available. ASTM shrinkage limit values were determined for all specimens to provide a standardised reference point; however, the full shrinkage curves are considered more informative for interpreting desiccation behaviour and stabilisation pathways.

Figures 3a and 3b present the laboratory data and the fitted curve showing void ratio and MC. The changes of dry density during desiccation are also shown.

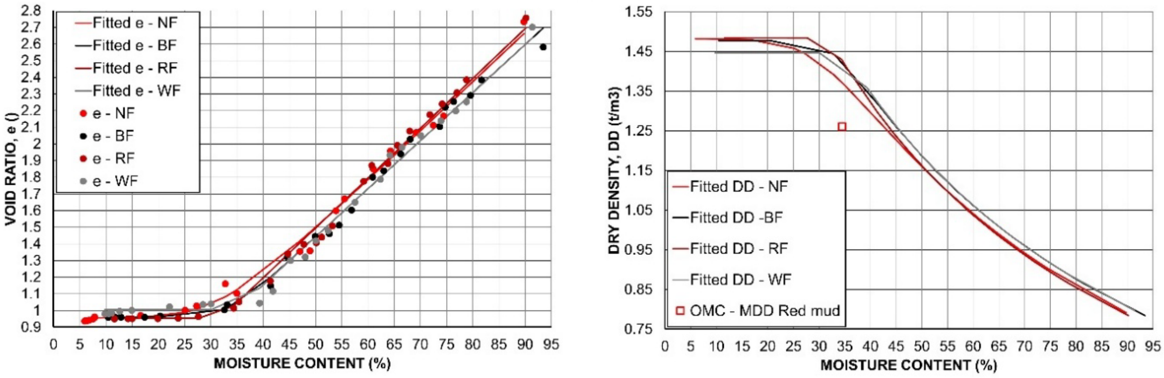

(a) (b)

Figure 3 Volumetric shrinkage tests for red mud with and without fibre reinforcement; (a) Moisture content versus fitted void ratios; (b) Moisture content versus calculated dry densities and optimum moisture content versus maximum dry density of red mud

Volumetric shrinkage testing indicates that fibre reinforcement influences the rate and pathway of void ratio reduction during desiccation of red mud. Fibres do not fundamentally alter the overall void ratio–MC relationship of red mud, with all specimens exhibiting similar behaviour at high MC values. This is validated by the volumetric shrinkage results following the ASTM D4943-25 test method. Volumetric shrinkage limit (SL) was approximately 31% on all specimens.

However, closer inspection of the fitting curves indicates a subtle but consistent divergence between unreinforced and fibre-reinforced specimens as drying progresses, predominantly at intermediate MC values. Red mud specimens with BF and WF exhibit a more rapid reduction in void ratio with decreasing MC compared with unreinforced red mud. For a given MC, these reinforced specimens consistently exhibit lower void ratios, indicating earlier fabric rearrangement and densification during drying. Similarly, the fitted shrinkage curves show a slightly earlier inflexion point, marking the transition from structural to residual shrinkage at higher MC values for all fibre-reinforced red mud specimens. Although the difference in voids compared to the unreinforced red mud is still within the same order of magnitude, having lower void ratios consistently starting from higher MC values is of great significance during long-term desiccation, which is the case when the material is contained in a TSF. This shows that fibre inclusion allows voids to enter the red mud matrix at higher MC values.

The evolutions of dry density displayed in Figure 4b support this interpretation. Overall, all specimens follow similar densification pathways during desiccation. However, BF- and WF-reinforced red mud tend to reach their asymptotic dry density at marginally higher moisture contents than the unreinforced material. This suggests that, for certain fibre geometries and surface characteristics, fibre inclusion can promote earlier stabilisation of the red mud fabric during drying.

Compared to standard compaction tests, with an external force imposing volumetric changes of a material to achieve a given MDD, the overall shrinkage of the samples achieved higher dry density values, closer to what can be achieved at a TSF if desiccation agents are constant and efficient.

The overall shrinkage demand remains governed by the mineralogical composition and fine-grained matrix of red mud, characterised by a high proportion of amorphous material and aluminosilicate and iron-rich phases with stronger water-retention capacity. These parameters are summarised in Table 1. Fibre reinforcement does not modify these intrinsic controls on shrinkage magnitude, rather, it influences the mechanical alteration of shrinkage, facilitating earlier void collapse and densification.

When considered alongside tensile strength and crack propagation results, these observations indicate that fibre reinforcement can assist red mud in reaching a stable, lower void ratio state with reduced desiccation, without significantly changing the total shrinkage experienced. This behaviour is favourable, as it implies a reduced drying requirement to achieve structural stabilisation and a lower propensity for shrinkage-induced cracking during closure and rehabilitation.

3.3 Mechanical test results

3.3.1 Preparation parameters

The key parameters controlled during the mechanical testing program, including UCS and BTS testing, were the dry mass of red mud, the mass of fibres and the mass of added water. All specimens were prepared at the adopted OMC and MDD of red mud of 34.5% MC and 1.26 t/m³, respectively, as determined from the standard compaction tests (Figure 2). Variability between specimens remained within ±5% of the target values, confirming acceptable repeatability and preparation consistency.

Following mixing, the prepared material was sealed and allowed to cure for a minimum of 24 hours prior to compaction. Specimens were then manually compacted using the sleeved tube and hammer in Figure 4. This compaction method was selected to ensure consistent energy input across specimens while minimising sample disturbance.

(a) (b)

Figure 4 Sample preparation for mechanical tests; (a) Plastic-reinforced red mud compacted sample for unconfined compressive strength test; (b) Steel case and hammer for preparation of samples for Brazilian tensile strength and unconfined compressive strength tests

The preparation procedure described by Hua (Tian et al. 2023) was followed for BTS specimens, with particular attention to prevent sample damage during sample extrusion. To reduce the risk of rupture, specimens were initially compacted at a reduced MC of approximately 12%, after which the remaining water required to reach the target OMC was applied by spraying. All specimens were weighed after each compaction stage to monitor mass consistency. MC tests were conducted at the conclusion of each mechanical test to quantify moisture loss.

UCS specimens were prepared with nominal dimensions of 70 mm diameter and 140 mm height, while BTS specimens were prepared with nominal dimensions of 100 mm diameter and 50 mm height. Fibre lengths were trimmed to a nominal maximum length not exceeding 10% of the specimen diameter to minimise potential boundary effects associated. The original fibre lengths are listed in Table 2.

3.3.2 Brazilian tensile strength test results

The BTS tests were conducted in 3 sub-groups or repetitions of specimens per sample type, prepared under the same specifications described in Section 3.3.1. In total, 12 tests were completed. Each test was terminated either at specimen rupture or at a displacement of 20 mm, by which stage the peak load had been clearly identified. Figure 5 summarises the displacement versus load responses obtained for each sample type.

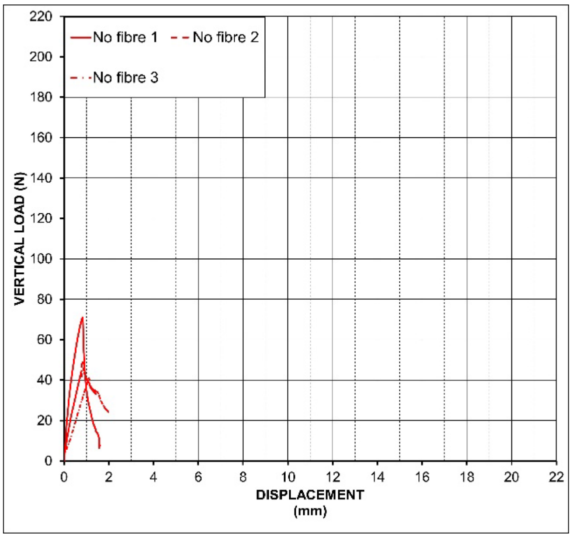

(a)

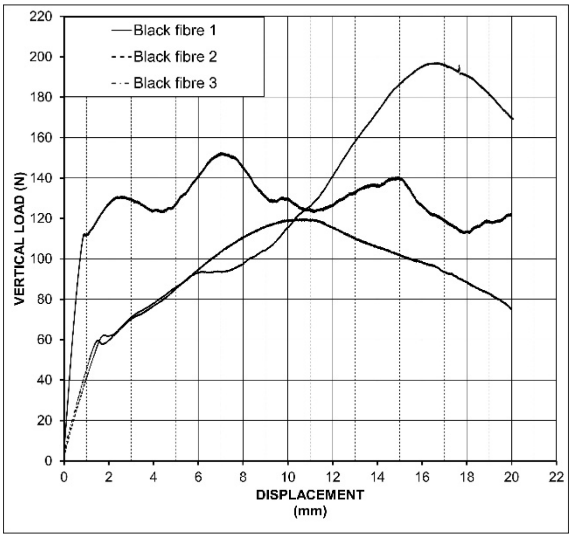

(b)

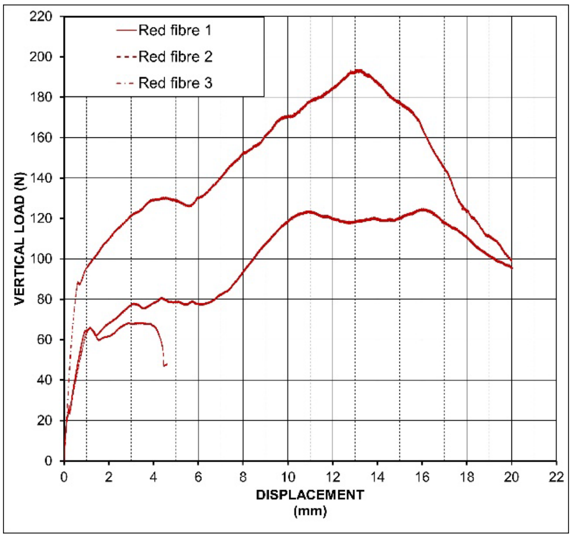

(c)

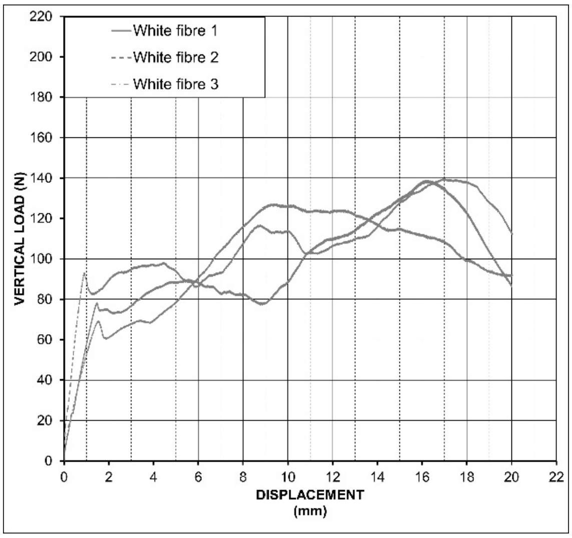

(d)

Figure 5 Brazilian tensile strength tests for red mud unreinforced and red mud reinforced with 1% fibre; (a) Red mud – no fibre (NF); (b) Red mud – BF; (c) Red mud – RF; (b) Red mud – WF

As expected, the unreinforced red mud exhibited very low load resistance prior to failure. Once the peak load was reached, the specimens rapidly lost their ability to sustain load, indicating a brittle, matrix-controlled tensile response with very low ductility. This behaviour is characteristic of fine-grained materials with low tensile capacity under indirect tension (Narvaez et al. 2015; Tian et al. 2024).

In contrast, all fibre-reinforced specimens displayed a clear inflexion in the load–displacement response at a displacement of approximately 1 mm, which was consistently observed across all fibre types. Beyond this point, the applied load continued to increase at varying rates, depending on fibre type, indicating a transition from matrix-dominated behaviour to fibre-controlled tensile resistance and evidencing a high to very high ductility compared to unreinforced red mud. Although some variability in peak load was observed between repetitions of the same fibre type, all reinforced specimens exhibited a broadly similar increasing post-inflexion trend and a peak load of 2–2.5 times the peak load of unreinforced red mud. Peak loads and calculated tensile strength values are summarised in Table 3. Unreinforced red mud specimens had an average tensile strength of 6.83 kPa, whereas BF-, RF- and WF-reinforced specimens had average values of 19.93 kPa, 16.44 kPa and 17.23 kPa, respectively.

These results indicate that crack initiation in the red mud matrix occurs at a similar displacement for both unreinforced and reinforced specimens. However, following crack initiation, the tensile resistance of the fibre-reinforced specimens is maintained and enhanced through fibre mobilisation and crack bridging mechanisms, allowing load transfer to continue until final failure.

Among the reinforced specimens, RF and BF generally achieved the highest peak loads, followed by WF specimens with a moderately higher peak load compared to the unreinforced material. However, BF and WF specimens exhibited more consistent post-peak load–displacement behaviour across replicates, suggesting a more uniform tensile response. These differences indicate that fibre type influences not only the magnitude of tensile resistance but also the stability and consistency of post-cracking behaviour.

3.3.3 Crack propagation on Brazilian tensile strength tests

Crack initiation and propagation during the BTS tests were captured using an ultra high-speed camera (Phantom v2011) operating at a recording rate of 100 frames per second. The camera was positioned behind the specimen to allow clear visualisation of crack development during loading.

Figure 6a displays the typical BTS set-up in the load frame using the camera alignment. All tests were recorded to allow frame to frame analysis of crack initiation and propagation. An example frame is presented in Figure 6b.

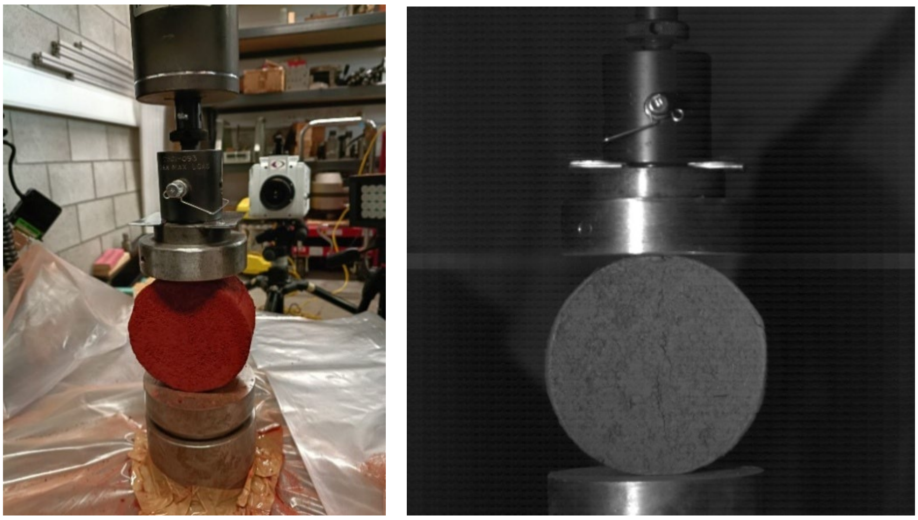

(a) (b)

Figure 6 Typical set-up and representative recorded frames for Brazilian tensile strength test using an ultra high-speed camera; (a) Red mud specimen set-up prior to testing; (b) Crack initiation example during Brazilian tensile strength test

High-speed imaging showed that fibre reinforcement specimens exhibited an overall delayed crack initiation, a larger resistance to load after crack initiation and more distributed cracking compared with unreinforced red mud, consistent with the improved tensile strength and post-cracking response observed in mechanical testing.

The timing between mechanical loading and image acquisition was synchronised with both the load frame and the camera recording initiated simultaneously. Following testing, the recorded sequences were converted from slow-motion playback to real-time units to determine the approximate time and displacement for the first visible crack and the crack configuration at peak applied load.

Table 3 summarises the BTS results together with the interpreted crack initiation and propagation mechanisms identified from data and the corresponding frames for all specimens.

Table 3 Test results of Brazilian tensile strength for red mud with and without fibre reinforcement

Sample name	Peak load, P_{peak} (N)	Tensile strength (kPa)	First crack load, P_{crack} (N)	Crack load ratio, P_{crack}/P_{peak}	Time to peak load, t_{peak} (s)	Time to first crack, t_{crack} (s)	Crack time ratio, t_{crack}/t_{peak}	Normalised tensile strength
NF 1	71.09	**9.05**	37.32	0.52	248.4	86.01	0.35	–
NF 2	48.83	**6.22**	22.45	0.46	52.4	25.43	0.49	–
NF 3	40.92	**5.21**	21.80	0.53	331.7	171.4	0.52	–
BF 1	152.69	**19.44**	122.98	0.81	420.20	102.82	0.24	3.68
BF 2	197.09	**25.09**	81.92	0.42	4,998.3	1,348.52	0.27	2.24
BF 3	119.90	**15.27**	57.89	0.48	647.1	99.97	0.15	2.85
RF 1	124.95	**15.91**	78.46	0.63	963.7	241.5	0.25	2.33
RF 2	68.44	**8.71**	65.53	0.96	203.4	66.82	0.33	1.28
RF 3	194.02	**24.70**	120.39	0.62	792.8	172.6	0.22	3.62
WF 1	138.87	**17.68**	75.06	0.54	969.1	106.04	0.11	2.59
WF 2	139.78	**17.80**	83.24	0.6	1,021.5	88.75	0.09	2.61
WF 3	127.42	**16.22**	61.63	0.48	560.9	75.01	0.13	2.38

3.3.4 Unconfined compressive strength test results

UCS tests were conducted on unreinforced and fibre-reinforced red mud specimens prepared in accordance to Section 3.3.1 to provide contextual information on compressive behaviour under low moisture conditions. While red mud exhibits a limited propensity to develop cementitious characteristics due to the presence of hematite and calcite in its mineralogical composition and despite the predominant presence of amorphous particles that might affect the overall red mud behaviour as shown in the minerals and quantities in Table 1 (Quintero et al. 2017), no external cementitious binder was added in this study. Consequently, any changes in compressive response can be attributed solely to mechanical interactions between the fibres and the red mud matrix.

Figure 7 present the stress–displacement responses obtained for fibre-reinforced red mud and unreinforced red mud. The unreinforced specimens exhibited low peak UCS values and a brittle post-peak response, characterised by rapid strength loss following failure. The average peak UCS of the unreinforced red mud was 77.8 kPa, which is consistent with the water content used and fine-grained nature of the material.

Fibre-reinforced specimens showed modest increases in peak UCS, with average values of 108.2 kPa, 100.9 kPa and 96.9 kPa for BF, RF and WF, respectively. However, the primary influence of fibre inclusion was not a substantial increase in peak compressive strength, but a pronounced enhancement in post-peak load retention and deformation capacity. All fibre-reinforced red mud specimens exhibited a more gradual post-peak softening response, indicating a transition from brittle, matrix-controlled failure to a more ductile, fibre-controlled compressive behaviour.

This behaviour is consistent with fibre reinforcement mechanisms in weak geomaterials, where fibres act to restrain crack propagation and maintain load transfer after matrix failure. From a TSF closure perspective, the enhanced post-peak deformation capacity observed in the UCS tests is particularly relevant, as it indicates improved tolerance to localised strain, cracking and heterogeneity without catastrophic loss of load-bearing capacity.

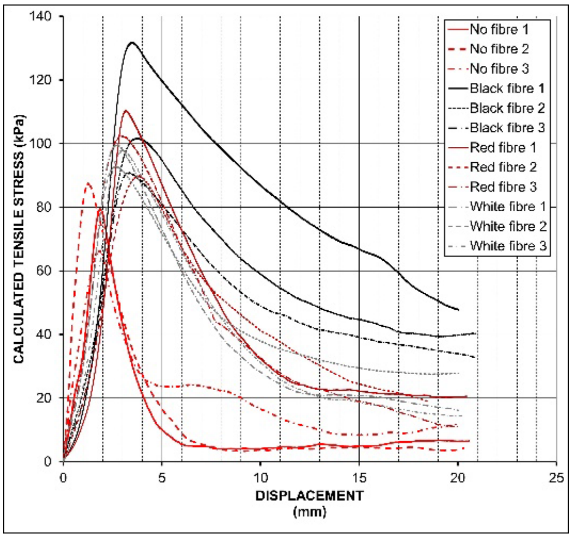

Figure 7 Stress displacement response from unconfined compressive strength tests for unreinforced red mud and plastic-reinforced red mud specimens prepared at optimum moisture content

3.3.5 Correlation between linear roughness and Brazilian tensile strength

The BTS results and crack propagation shown in sections 3.3.2 and 3.3.*3* demonstrate the transition from brittle tensile behaviour of unreinforced red mud to a more ductile, fibre-controlled response. All fibre types exhibited tensile strengths well above the stresses found on BTS testing (Table 2), indicating that specimen behaviour was governed by a fibre–matrix interaction and pull-out resistance rather than fibre rupture. While peak BTS is influenced by fibre stiffness, geometry and crack bridging efficiency, fibre roughness contributes to post-cracking resistance and display fibres ability to maintain matrix integrity.

To investigate this mechanism, the average R_a of each fibre (Table 2*)* was incorporated into the analysis. Under tensile loading, rougher fibre surfaces enhance crack bridging efficiency and allowing tensile stresses to be sustained beyond matrix cracking.

On this basis, correlations between fibre R_a and BTS were examined to evaluate the contribution of fibre asperities to post-cracking tensile behaviour independently of the intrinsic strength of the red mud matrix. BTS results for fibre-reinforced specimens were normalised relative to the mean BTS of unreinforced red mud using Equation 1, with the individual and average values presented in Table 3. This normalisation isolates the tensile contribution of fibre reinforcement while reducing specimen variability.

$$Normlised\ NTS = \frac{\sigma_{t,reinforced}}{\overline{\sigma_{t,NF}}} \quad (1)$$

where:

$\sigma_{t,\ reinforced}$	=	tensile strength for each fibre-reinforced specimen
$\overline{\sigma_{t,NF}}$	=	mean tensile strength for red mud specimens with no fibre, NF.

Figure 8 presents the relationship between normalised BTS and the average R_a, including individual test results and average values with standard deviation. The results indicate a systematic increase in normalised tensile strength with increasing R_a. This is consistent with fibre–matrix interaction mechanisms where roughness enhances interlocking and pull-out resistance, thereby improving crack bridging efficiency (Shaia & Abuel-Naga 2014; Tang et al. 2016).

This relationship should be interpreted as indicative rather than definitive. However, it provides mechanistic support for the role of fibre surface characteristics in governing tensile resistance and crack control in fibre-reinforced red mud under desiccation-relevant conditions.

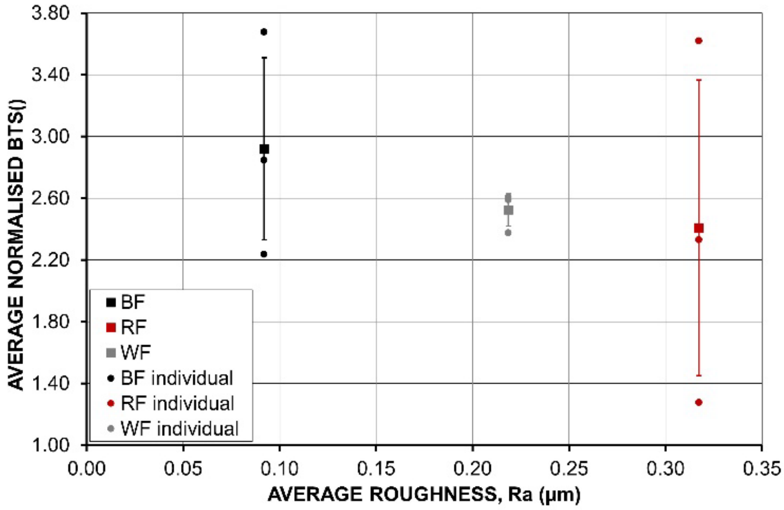

Figure 8 Fibre average roughness versus average normalised Brazilian tensile strength for plastic-reinforced red mud

The results shown in Figure 8 demonstrate that reinforced red mud's reaction to tensile strength cannot be attributed to roughness alone. Out of all fibres, BF – which has the lowest average roughness – provided the highest peak BTS, demonstrating that increased roughness does not directly correspond to higher tensile strength. Instead, the peak resistance is governed by the combination of parameters such as fibre composition, stiffness, geometry and early crack bridging prior to significant pull-out. Other factors contributing tensile resistance could also be the MC in the mix to generate apparent cohesion and red mud particles' shape and geometry interacting with fibres.

WF specimens exhibited the most consistent tensile performance, indicating a more uniform fibre–red mud interaction and more stable tensile resistance. The high variability observed in RF-reinforced red mud reflects the increased sensitivity to rougher fibres to specimen-scale dispersion and crack path development. These findings highlight the multiple metrical nature of fibre reinforcement in red mud.

4 Conclusion

The present study assessed the effect of plastic fibre reinforcement on red mud behaviour at moisture conditions representative of TSF closure. While practical implementation of fibre addition within TSFs remains a challenge, this study highlights the potential of fibre reinforcement as an alternative material enhancement approach for improving strength, shrinkage behaviour and long-term stability, while also evidencing a potential economic and operational benefit of having 2 waste streams (plastic and mining waste) into a TSF.

The key conclusions are summarised below:

- Fibre reinforcement significantly increased tensile strength, with average BTS values approximately 2–2.5 times higher than unreinforced red mud. This corresponds to an increase of approximately 192%, 141% and 152% for BF, RF and WF, respectively.
- Compressive strength also improved, with average UCS increases of approximately 39%, 30% and 25% for BF-, RF- and WF-reinforced red mud, respectively. However, the primary benefit of fibre addition was enhanced post-peak load retention rather than peak strength gain.

- Volumetric shrinkage results indicate that fibre reinforcement promotes earlier densification during drying. Void ratio reductions of approximately 2–6% at LL conditions and 5–7% at SL conditions were observed for fibre-reinforced specimens compared with unreinforced red mud. This may contribute to reduced storage volume requirements in TSFs.
- Fibres act as a mechanical binding agent within the red mud matrix. Fibres improve post-peak displacement and transition failure from brittle to ductile, by delaying failure, controlling crack propagation and sustaining load transfer after crack initiation.
- The average time from first crack to peak load in BTS tests increased from 116.6 s for unreinforced red mud to 1504.8 s, 493.0 s and 760.6 s for BF, RF and WF, respectively. This represents an increase in post-crack load bearing duration of approximately 13, 4.2 and 6.5 times, respectively. This enhanced crack control is particularly relevant for TSF applications, as sustained load transfer after crack initiation may allow infiltration of water (e.g. rainfall or subsequent deposition layers) while maintaining structural integrity, supporting more controlled desiccation and matrix stability.
- Fibre reinforcement modifies long-term shrinkage behaviour by promoting earlier stabilisation and reducing crack-controlled desiccation pathways, without significantly increasing the overall density or shrinkage magnitude, thus potentially reducing the used volume at a given TSF.
- Surface fibre roughness contributed to enhance pull-out resistance. However, peak tensile strength is influenced by a series of factors such as fibre roughness, geometry and stiffness.
- WF exhibited the most consistent tensile performance, while BF achieved the highest peak tensile resistance despite lower surface roughness. RF had a similar maximum peak resistance but greater variability, reflecting sensitivity to fibre dispersion and crack path development.
- Overall, fibre reinforcement provides a viable strategy to improve red mud shrinkage, crack control, tensile and compressive performance and overall structural integrity with red mud under desiccation conditions relevant to TSF closure.
- Further investigation is recommended to assess fibre performance under a larger MC range and cyclic wetting and drying conditions. Evaluating practical implementation methods for fibre incorporation in field-scale TSF operations is also recommended.

Acknowledgement

The authors would like to acknowledge Texo ReoCo (now ENVIROMESH) for supplying the plastic fibre prototypes used in this study, in particular, Alex Lester, Stuart Neilson and Gillis Broinowski who provided insight about plastic fibres.

The authors also want to acknowledge the services provided by Wael Al Abdulla and his team from the Australian National Fabrication Facility (Qld Node) on the SEM and fibre roughness tests.

References

Arredondo, E, Suazo, G & Araya, V 2020, 'Surface cracking in thickened tailings: mechanisms and its influence on evaporation and water contents', in H Quelopana (ed.), *Paste 2020: 23rd International Conference on Paste, Thickened and Filtered Tailings*, Gecamin Publications, Santiago, https://doi.org/10.36487/ACG_repo/2052_103

Australian Government 2016, *Tailings management*, Canberra.

Bai, X, Xue, H, Song, Z, Dai, J, Kan, Z & Wang, J 2026, 'Research on the early crack resistance and abrasion resistance of concrete with graphite tailings and basalt fiber', *Case Studies in Construction Materials*, vol. 24, https://doi.org/10.1016/J.CSCM.2026.E05934

Chaduvula, U, Viswanadham, BVS & Kodikara, J 2017, 'A study on desiccation cracking behavior of polyester fiber-reinforced expansive clay', *Applied Clay Science*, vol. 142, https://doi.org/10.1016/J.CLAY.2017.02.008

Chen, X, Shi, X, Zhang, S, Chen, H, Zhou, J, Yu, Z & Huang, P 2020, 'Fiber-reinforced cemented paste backfill: The effect of fiber on strength properties and estimation of strength using nonlinear models', *Materials*, vol. 13, no. 3, https://doi.org/10.3390/MA13030718

Consoli, NC, Prietto, PDM & Ulbrich, LA 1999, 'The behaviour of a fibre-reinforced cemented soil', *Proceedings of the Institution of Civil Engineers - Ground Improvement*, vol. 3, no. 1, pp. 21–30, https://doi.org/10.1680/GI.1999.030103

Cristelo, N, Cunha, VMCF, Topa Gomes, A, Araújo, N, Miranda, T & Lurdes Lopes, MD 2017, 'Influence of fibre reinforcement on the post-cracking behaviour of a cement-stabilised sandy-clay subjected to indirect tensile stress', *Construction and Building Materials*, vol. 138, pp. 163–173, https://doi.org/10.1016/J.CONBUILDMAT.2017.02.010

Festugato, L, Consoli, NC & Fourie, A 2015, 'Cyclic shear behaviour of fibre-reinforced mine tailings', *Geosynthetics International*, vol. 22, no. 2, pp. 196–206, https://doi.org/10.1680/gein.15.00005

Fredlund, DG, Rahardjo, H & Fredlund, MD 2006, 'Unsaturated soil mechanics in engineering practice', *Journal of Geotechnical and Geoenvironmental Engineering*, vol. 132, no. 3, 286–321, https://doi.org/10.1002/9781118280492

Girao, JMS & Casagrande, MDT 2019, 'Evolución de los parámetros de resistencia y comportamiento volumétrico de un relave de hierro reforzado con fibras de polipropileno en la condición no drenada' (Strength parameters evolution and volumetric behaviour of polypropylene fibre reinforced iron tailings under undrained conditions), *XVI Pan-American Conferences on Soil Mechanics and Geotechnical Engineering (PCSMGE)*, pp. 1786–1795, https://www.issmge.org/publications/publication/evolucion-de-los-parametros-de-resistencia-y-comportamiento-volumetrico-de-un-relave-de-hierro-reforzado-con-fibras-de-polipropileno-en-la-condicion-no-drenada

Girao, JMS, Casagrande, MDT & Barragán, LYR 2019, 'Comportamiento volumétrico y evolución de los parámetros de resistencia de relaves de oro reforzados con fibra de polipropileno homogéneamente distribuida' (Volumetric behaviour and strength parameters evolution of homogeneously distributed polypropylene fibre reinforced gold tailings), *XVI Pan-American Conference on Soil Mechanics and Geotechnical Engineering (XVI PCSMGE)*, pp. 1796–1803, https://www.issmge.org/publications/publication/comportamiento-volumetrico-y-evolucion-de-los-parametros-de-resistencia-de-relaves-de-oro-reforzados-con-fibra-de-polipropileno-homogeneamente-distribuida

Guo, Z, Qiu, J, Kirichek, A, Zhou, H, Liu, C & Yang, L 2024, 'Recycling waste tyre polymer for production of fibre reinforced cemented tailings backfill in green mining', *Science of The Total Environment*, vol. 908, https://doi.org/10.1016/J.SCITOTENV.2023.168320

Kodikara, J & Costa, S 2013, 'Desiccation cracking in clayey soils: Mechanisms and modelling', *Multiphysical Testing of Soils and Shales* Springer, Heidelberg, https://doi.org/10.1007/978-3-642-32492-5_2

Liu, J, Yang, H, Zhang, D, Wang, Y, Xiao, W, Ye, C, Zheng, B & Yang, Y 2021, 'Mechanical and permeation response characteristics of basalt fibre reinforced tailings to different reinforcement technologies: An experimental study', *Royal Society Open Science*, vol. 8, no. 9, https://doi.org/10.1098/rsos.210669

Luckeneder, S, Giljum, S, Schaffartzik, A, Maus, V & Tost, M 2021, 'Surge in global metal mining threatens vulnerable ecosystems', *Global Environmental Change*, vol. 69, https://doi.org/10.1016/J.GLOENVCHA.2021.102303

Luo, Y, Zhang, J, Zhou, Z, Aguilar-Lopez, JP, Greco, R & Bogaard, T 2023, 'Effects of dynamic changes of desiccation cracks on preferential flow: Experimental investigation and numerical modeling', *Hydrology and Earth System Sciences*, vol. 27, no. 3, https://doi.org/10.5194/HESS-27-783-2023

Martinez, A & Frost, JD 2017, 'The influence of surface roughness form on the strength of sand–structure interfaces', *Géotechnique Letters*, vol. 7, no. 1, pp. 104–111, https://doi.org/10.1680/jgele.16.00169

Mishra, PN, Scheuermann, A, Bore, T & Li, L 2019, 'Salinity effects on soil shrinkage characteristic curves of fine-grained geomaterials', *Journal of Rock Mechanics and Geotechnical Engineering*, vol. 11, no. 1, pp. 181–191, https://doi.org/10.1016/J.JRMGE.2018.06.008

Narvaez, B, Aubertin, M & Saleh-Mbemba, F 2015, 'Determination of the tensile strength of unsaturated tailings using bending tests', *Canadian Geotechnical Journal*, vol. 52, no. 11, https://doi.org/10.1139/CGJ-2014-0156

Olaya, SQ, Williams, DJ, Zhang, C, Llano-Serna, M & Silva, GG 2023, 'Analysis of the geotechnical characteristics of fibre reinforced tailings', *Mine waste and Tailings Conference Proceedings*, The Australasian Institute of Mining and Metallurgy, Melbourne, pp. 91–109.

Olaya, SQ, Zhang, C, Williams, DJ, Lei, X, Zhao, Z & Llano-Serna, M 2020, 'Use of high-performance fibres to enhance tailings', *Tailings and Mine Waste 2020*, UBC Studios, The University of British Columbia, Vancouver, pp. 328–337.

Pradhan, G, Tripathy, B, Ram, DK, Digal, AK & Das, AP 2024, 'Bauxite mining waste pollution and its sustainable management through bioremediation', *Geomicrobiology Journal*, vol. 41, no. 4, pp. 335–344, https://doi.org/10.1080/01490451.2023.2235353

Quintero, S, Durante, M, Serati, M & Williams, DJ 2017, 'Geotechnical characterisation of neutralised red mud for use in civil engineering construction and manufacturing', *Proceedings of the 32nd International Conference on Solid Waste Technology and Management*, pp. 613–623.

Ranabhat, A, Zhang, C, Quintero Olaya, S & Williams, DJ 2023, 'Farming method and assessment of its application in bauxite residue using a scaled laboratory model', *Mine Waste and Tailings Conference 2023: Conference Proceedings*, The Australasian Institute of Mining and Metallurgy, Melbourne, pp. 589–597.

Ranabhat, A, Zhang, C, Quintero Olaya, S & Williams, DJ 2025, 'Dewatering behaviour of filtered red mud', *Life of Mine / Mine Waste and Tailings Conference 2025: Conference Proceedings*, The Australasian Institute of Mining and Metallurgy, Melbourne, pp. 773–788.

Shaia, HA & Abuel-Naga, HM 2014, 'On the normalized relative roughness for soil-fiber reinforced polymer interface shear behaviour', *Lowland Technology International*, vol. 16, no. 1, pp. 9–13, https://doi.org/10.14247/LTI.16.1_9

Stakne, K, Smole, MS, Kleinschek, KS Jaroschuk, A & Ribitsch, V 2003, 'Characterisation of modified polypropylene fibres', *Journal of Materials Science*, vol. 38, pp. 2167–2169.

Svobodova-Sedlackova, A, Calderón, A, Fernandez, AI, Chimenos, JM, Berlanga, C, Yücel, O, Barreneche, C & Rodriguez, R 2024, 'Mapping the research landscape of bauxite by-products (red mud): an evolutionary perspective from 1995 to 2022', *Heliyon*, vol. 10, no. 3, https://doi.org/10.1016/J.HELIYON.2024.E24943

Tang, C-S, Wang, D-Y, Cui, Y-J, Shi, B & Li, J 2016, 'Tensile strength of fiber-reinforced soil', *Journal of Materials in Civil Engineering*, vol. 28, no. 7, https://doi.org/10.1061/(ASCE)MT.1943-5533.0001546

Thomason, J 2023, 'The influence of fibre cross section shape and fibre surface roughness on composite micromechanics', *Micro*, vol. 3, no. 1, pp. 353–368, https://doi.org/10.3390/micro3010024

Tian, H, David J, W, Keith, M, Chenming, Z, Sebastian Quintero, O, Wenqiang, Z & Tang, C 2023, 'Engineering properties of fine-grained red mud', *International Journal of Mining, Reclamation and Environment*, vol. 37, no. 6, pp. 399–418, https://doi.org/10.1080/17480930.2023.2212575

Tian, H, Williams, DJ & Mandisodza, K 2024, 'Tensile strength and dilative characteristics of compacted unsaturated clay-sized metalliferous tailings for bulk earthworks', *Bulletin of Engineering Geology and the Environment*, vol. 83, no. 9, https://doi.org/10.1007/S10064-024-03860-1

Vangla, P & Latha Gali, M 2016, 'Effect of particle size of sand and surface asperities of reinforcement on their interface shear behaviour', *Geotextiles and Geomembranes*, vol. 44, no. 3, pp. 254–268, https://doi.org/10.1016/J.GEOTEXMEM.2015.11.002

Vo, TD, Pouya, A, Hemmati, S & Tang, AM 2019, 'Modelling desiccation crack geometry evolution in clayey soils by analytical and numerical approaches', *Canadian Geotechnical Journal*, vol. 56, no. 5, https://doi.org/10.1139/CGJ-2018-0105

Williams, DJ 2015, 'Placing soil covers on soft mine tailings', in B Indraratna & J Chu (eds), *Ground Improvement Case Histories: Compaction, Grouting and Geosynthetics*, Elsevier Inc., Amsterdam, pp. 51–81.

Williams, DJ 2021, 'Lessons from tailings dam failures—where to go from here?', *Minerals*, vol. 11, vol. 11, no. 8, https://doi.org/10.3390/MIN11080853

Wu, D, Wang, C, Liu, H, Liu, X, Wang, H & Wang, Q 2024, 'Recycled polyester fiber reinforcing red mud-improved volcanic ash as a sustainable construction material', *Construction and Building Materials*, vol. 413, https://doi.org/10.1016/J.CONBUILDMAT.2023.134821

Yi, XW, Ma, GW & Fourie, A 2015, 'Compressive behaviour of fibre-reinforced cemented paste backfill', *Geotextiles and Geomembranes*, vol. 43, no. 3, 207–215, https://doi.org/10.1016/J.GEOTEXMEM.2015.03.003

Zafar, T, Ansari, MA & Husain, A 2023, 'Soil stabilization by reinforcing natural and synthetic fibers – a state of the art review', *Materials Today: Proceedings*, Elsevier https://doi.org/10.1016/J.MATPR.2023.03.503

Zhang, W, Zhang, C, Lei, X, Olaya, SQ, Zhu, Y & Williams, DJ 2025, 'Performance assessment of a monolithic soil cover over hypersaline bauxite residue under natural weather conditions', *Engineering Geology*, vol. 353, https://doi.org/10.1016/J.ENGGEO.2025.108120

Zhang, W, Zhang, C, Lei, X, Zhu, Y, Quintero, S, Williams, DJ & O'neill, M 2019, 'Assessing salt migration from compacted bauxite residual into overlying cover using an instrumented column', *Proceedings of Tailings and Mine waste 2019*, The University of British Columbia, Vancouver, pp. 309–318.

Zollo, RF 1997, 'Fiber-reinforced concrete: an overview after 30 years of development', *Cement and Concrete Composites*, vol. 19, no. 2, pp. 107–122, https://doi.org/10.1016/S0958-9465(96)00046-7

Zou, S, Gao, Y, Zhou, Y, Sun, H, Yang, Z, Yang, C & Jiang, H 2025, 'Study on the multi-scale tensile mechanical behavior of fiber reinforced cemented tailings backfill considering surface roughness effects', *Construction and Building Materials*, vol. 462, https://doi.org/10.1016/J.CONBUILDMAT.2025.139988